ORIGINAL ARTICLE

Discovery of a potent PROTAC degrader for RNA demethylase FTO as antileukemic therapy

Lu Liu[a,b,†], Yuanlai Qiu[a,c,†], Yuying Suo[b,c,†], Siyao Tong[a,c],
Yiqing Wang[a,c], Xi Zhang[a,c], Liang Chen[b], Yue Huang[a,b],
Huchen Zhou[d], Hu Zhou[a,b,c,*], Ze Dong[a,c,*], Cai-Guang Yang[a,b,c,d,e,*]

[a]School of Pharmaceutical Science and Technology, Hangzhou Institute for Advanced Study, University of Chinese Academy of Sciences, Hangzhou 310024, China
[b]State Key Laboratory of Drug Research, Shanghai Institute of Materia Medica, Chinese Academy of Sciences, Shanghai 201203, China
[c]University of Chinese Academy of Sciences, Beijing 100049, China
[d]State Key Laboratory of Microbial Metabolism, School of Pharmacy, Shanghai Jiao Tong University, Shanghai 200240, China
[e]Shandong Laboratory of Yantai Drug Discovery, Bohai Rim Advanced Research Institute for Drug Discovery, Yantai 264117, China

Abstract   The fat mass and obesity-associated protein (FTO) is an RNA demethylase required for catalytic demethylation of N^6-methyladenosine (m^{6}A); it is highly expressed and functions as an oncogene in acute myeloid leukemia (AML). Currently, the overarching objective of targeting FTO is to precisely inhibit the catalytic activity. Meanwhile, whether FTO degradation also exerts antileukemic effects remains unknown. Herein, we designed the first FTO-targeting proteolysis targeting chimera (PROTAC) degrader QP73 using our FTO inhibitor Dac85—which potently inhibits FTO demethylation in AML cell lines—as a warhead. Notably, QP73 significantly induced FTO degradation in a time-, dose-, and ubiquitin−proteasome system-dependent manner and had superior antiproliferative activities to the FTO inhibitor Dac85 in various AML cell lines. Moreover, QP73 treatment significantly increased m^{6}A modification on mRNA, promoted myeloid differentiation, and induced apoptosis of AML cells. Quantitative proteomics analysis showed that QP73 induced complete FTO degradation, upregulating RARA and ASB2 abundance and downregulating CEBPA, MYC, PFKP, and LDHB levels in AML cells.

Lastly, QP73 exhibited antileukemic activity by increasing m^{6}A modification and decreasing FTO levels in xenograft AML tumors. This proof-of-concept study shows that FTO-targeting PROTAC degraders can regulate the FTO signaling pathway and have potential antileukemia applications.

1. Introduction

The decoration of RNA with N^6-methyladenosine (m^{6}A) is a dynamic and reversible posttranscriptional modification regulated by RNA-modifying enzymes[1,2], including methyltransferases (METTL3/METTL14 complex, METTL16, and METTL1), demethylases (FTO and ALKBH5), and reader proteins (such as YTH domain-containing proteins)[3]. The m^{6}A modification influences nearly every RNA metabolism step and broadly affects gene expression at multiple levels, thereby affecting various physiological and pathological processes[4]. FTO demethylation dysregulation results in m^{6}A homeostasis loss and causes diseases such as acute myeloid leukemia (AML)[5,6]. High FTO expression in AML cells promotes oncogene-mediated cell transformation and leukemogenesis. Therefore, FTO is a promising therapeutic target in antileukemia drug discovery.

Currently, the overarching objective of targeting FTO is to precisely inhibit FTO demethylation, in order to regulate the expression of downstream genes in AML cells[7−11]. In a previous proof-of-concept study showing that chemicals could regulate m^{6}A modification on mRNA in cells, we identified rhein as the first substrate-competitive FTO inhibitor[12]. Although rhein lacks selectivity, we found that meclofenamic acid (MA) selectively inhibited FTO rather than ALKBH5, paving the way for the rational design and sustained development of MA derivatives as selective and potent FTO inhibitors[8,13−14]. Among them, FB23-2 inhibited the proliferation of the primary AML cells and prolonged the survival of mice with a patient-derived AML xenograft[15,16]. Mechanistically, FB23-2 directly targeted FTO in AML cells, upregulated *ASB2* and *RARA* transcription, and downregulated *MYC* and *CEBPA* transcription, and suppressed functional leukemia stem cells. Others also performed a structure-based virtual screening and found that CS1/bisantrene and CS2/Brequinar exhibited strong antitumor effects in mouse models of AML and relapsed AML[17]. Recently, the natural product saikosaponin D demonstrated broad suppression of AML cell proliferation and apoptosis promotion, overcoming FTO-mediated leukemia resistance to tyrosine kinase inhibitors[18]. These inhibitors have paved the way toward investigating FTO's druggability as an antileukemia therapeutic target.

Besides inhibiting FTO demethylation, some FTO inhibitors also downregulated FTO in tumor cells. *R*-2HG inhibited FTO demethylation and downregulated the transcription of *CEBPA*[19]. Interestingly, suppressing *CEBPA* transcription substantially decreased *FTO* transcription in AML cells. This feedback pathway might also explain why the FTO inhibitor Dac51 similarly downregulated the FTO abundance in solid tumor cells[20]. Inspired by these observations, we propose that the rapid degradation of the FTO protein also represents a promising antileukemia strategy that proteolysis targeting chimeras (PROTACs) can achieve[21,22].

Compared with traditional inhibitors, PROTACs work at substoichiometric receptor occupancies and are more potent[23−27].

In this work, we report the discovery of QP73, a first-in-class PROTAC degrader for the RNA demethylase FTO which efficiently induced the FTO protein degradation in a dose-, time-, cereblon (CRBN)-, and proteasome-dependent manner in AML cells with various genetic backgrounds. Additionally, QP73 exhibited much superior antiproliferative activity to the FTO inhibitor Dac85, and showed therapeutic effects in an AML xenograft mouse model.

2. Materials and methods

2.1. Protein extraction and Western blot assay

The AML cells were lysed with RIPA buffer (Beyotime, P0013C) on ice for 20 min with protease inhibitor cocktail (Sangon Biotech, C600387-0001). After centrifugation at 15,000 rpm at 4 °C for 20 min, the supernatants were collected and quantified with the BCA protein assay kit (Beyotime, P0011). The sample was diluted with 5 × loading buffer and denaturized at 100 °C for 8 min, and then loaded to the 12% SDS-PAGE. The proteins were transferred onto nitrocellulose membrane (Millipore) and blocked with 5% skim milk, then incubated with antibodies against FTO (Abcam, ab124892), c-MYC (Abcam, ab32072), CRBN (Proteintech, 28494-1-AP), RARA (Beyotime, AF2398), ASB2 (ABcolonal, A17923), CEBPA (ABcolonal, A0904), LDHB (Beyotime, AF7365), PFKP (ABcolonal, A20983), GAPDH (ABcolonal, AC001), β-actin (Proteintech, 66009-1-Ig). HRP-conjugated Goat Anti-mouse (Cwbio, CW0102) or Anti-rabbit IgG (Cwbio, CW0103) was used as the secondary antibody. The membranes were visualized using the ECL detection system (CLINX ChemiScopeS6).

2.2. Inhibition of the demethylase activity in vitro in a dot blot assay

Single-stranded RNA (ssRNA) with m^{6}A modification was synthesized by Takara with the sequence of 5′-AUUGUCA(m^{6}A)CAGCAGC-3′. Demethylation activity assays were conducted in a 20 μL reaction mixture containing 50 mmol/L of HEPES buffer (pH 7.0), 2 μmol/L ssRNA, 200 nmol/L FTO, 283 mmol/L $(NH_4)_2(SO_4)_2 \cdot 6H_2O$, 75 mmol/L α-KG, 2 mmol/L L-ascorbic acid, 50 mg/mL BSA, and compound at indicated concentrations. The reactions were incubated at 37 °C for 2 h and quenched by the addition of 5 mmol/L EDTA followed by inactivation of FTO heating at 95 °C for 5 min. The ssRNA was precipitated and resuspended with RNase-free water, and subjected to the dot blot procedure to detect m^{6}A abundance.

2.3. Thermal shift assay

A thermal shift assay was performed with a Bio-Rad 96 system (Bio-Red, CFx 96 Touch). A mixture containing 2 μmol/L recombinant FTO protein or CRBN protein (AntibodySystem, EHK60701), 5 × SYPRO orange dye (Invitrogen, S6651), 50 mmol/L Tris-HCl (pH 7.5), 150 mmol/L NaCl, and compound at a concentration as indicated was heated from 35 to 95 °C at a 1% increment. The fluorescence intensity was detected at the excitation wavelength of 492 nm and the emission wavelength of 610 nm. The normalized T_m data were calculated by GraphPad Prism 8.3.0 software.

2.4. Cell cultures

NB4, MOLM13, HEL, and NOMO1 cells were cultured in RPMI 1640 medium supplemented with 10% fetal bovine serum (FBS) (Gibco, 10091148). MV4-11 and KG-1 cells were cultured in Iscove's modification of Dulbecco's medium supplemented with 10% FBS. MONOMAC6 cells were cultured in RPMI 1640 medium supplemented with 10% FBS, 1% NEAA (Thermo Fisher, 11140035) and 1% insulin (Gibco). The cells were maintained at 37 °C in 5% CO_2, and all cell lines were verified to be negative for mycoplasma using PCR analysis every two months.

2.5. Cell viability assay

Cell viability was determined using Cell Counting Kit-8 reagent (CCK8, Meilunbio, MA0218). The cells were seeded in 96-well plates at 5000 cells/well and treated with compounds at indicated concentrations or DMSO for 72 h. After treatment, 10 μL CCK8 reagent was added to each well and incubated at 37 °C for 4 h in 5% CO_2, then the absorbance was read at 450 nm with a microplate reader. The data were processed with GraphPad Prism 8.3.0 software. The IC_{50} values were calculated by GraphPad Prism 8.3.0 software using a log(agonist) vs. normalized response-variable slope model from three biological replicates.

2.6. Cellular thermal shift assay (CETSA)

NB4 and MV4-11 cells were collected and washed three times with PBS supplemented with protease inhibitor cocktail. Then the cells were subjected to three freeze-thaw cycles with liquid nitrogen and centrifuged at $20,000 \times g$ at 4 °C for 20 min. The cell lysis was treated with 50 μmol/L QP73 or DMSO for 30 min, and then equally divided into 200 μL tubes. The samples were heat shocked with a Thermal Cycler for 3 min and immediately cooled down to room temperature for another 3 min. Lastly, all samples were boiled and subjected to Western blot analysis.

2.7. Flow cytometry analysis

Cell apoptosis was validated with Annexin V-FITC/PI Apoptosis Detection Kit (KeyGEN BioTECH, KGA108-2) according to the manufacturer's protocol. NB4 and MV4-11 cells were collected and then washed twice with PBS. 5×10^5 cells/mL were resuspended in 500 μL of $1 \times$ binding buffer, following by adding the 5 μL Annexin V-FITC and 5 μL propidium iodide (PI). After a mild vortex, cells were incubated at room temperature for 15 min in the dark. Then each sample was determined by flow cytometry within 1 h with a Bio-Rad ZE5 and the annexin V-positive cells

were calculated with the FlowJo_V10 software. The statistical differences were analyzed using one-way ANOVA with Dunnett's multiple comparisons test.

Cell differentiation analysis with surface markers was conducted as described previously with some modifications[19]. NB4 and MV4-11 cells were utilized to induce myeloid differentiation by 200 nmol/L retinoic acid (Sigma−Aldrich, 223018) for 48 h, coupled with QP73 at indicated concentrations or DMSO. The induced AML cells were collected and washed with chilled PBS for three times, then stained with PE-conjugated anti-CD11b (eBioscience, 12-0118-42) and APC-conjugated anti-CD14 (eBioscience, 17-0149-42) at 4 °C for 30 min before subjected to flow cytometry analysis. The CD14- and CD11b-positive cells were calculated with the FlowJo_V10 software, and the statistical differences were analyzed using one-way ANOVA with Dunnett's multiple comparisons test.

2.8. Clone formation assay

MethoCult H4100 clone formation medium (STEMCELL Technologies, 04100) was mixed with IMDM medium and 10% FBS, then 1000 NB4 cells were added into the medium and seeded in 6-well plates at a density of 1000 cell/mL. After the addition of DMSO or QP73 at indicated concentrations, the cells were incubated at 37 °C in 5% CO_2 for 7 days and 200 μL culture medium was added into each well every 3 days. The cells were stained with 200 μL nitroblue tetrazolium chloride solution (Sigma−Aldrich, N5514-10TAB) (1 mg/mL) for 6 h, and the clones were then imaged with Leica DM2700 M.

2.9. RNA extraction, cDNA synthesis, and quantitative PCR (qPCR)

Total RNA samples were isolated with Trizol reagent following the manufacturer's guidelines. For cDNA synthesis, 1 μg total RNA samples were used for reverse transcription in 20 μL reaction volume using the Hiscript III Reverse Transcriptase (R302-01, Vazyme). The qPCR was performed with ChamQ Universal SYBR qPCR Master Mix (Vazyme, Q711-02) in equipment of Bio-Rad CFX96 Touch. GAPDH was used as endogenous control and each reaction was run in triplicates. The primers F-CCAGAACCTGAGGAGAGAATGG and R-CGATGTCTGTGAGGTCAAACGG were used for FTO, and F-TCAACGACCACTTTGTCAAGCTCA and R-GCTGGTGG TCCAGGGGTCTTACT for GAPDH.

2.10. Dot blot assay

For m^6A detection, total RNA was isolated with Trizol reagent and the poly (A)+ RNA was further enriched with Dynabeads mRNA direct purification kit (ThermoFisher, 61012) following the manufacturer's instructions. The RNA samples were denatured and loaded to the Immobilon-Ny+ membrane (Millipore, INYC00010) with a Bio-Dot Apparatus (Bio-Rad, #170-6545), and cross-linked onto the membrane with UV irradiation. After blocked with 5% nonfat milk for 1 h, the membrane was incubated with the specific anti-m^6A antibody (Cell Signaling Technology, 56593) at 4 °C overnight. Lastly, the membrane was then incubated with the HRP-conjugated goat anti-rabbit IgG (CoWin Biosciences, CW0103S) and developed with an ECL detection system (CLINX ChemiScopeS6). The loading control was established through staining of the membrane by 0.1% Methylene Blue (MB).

2.11. Lentivirus production and infection

Lentivirus for shFTO-1, shFTO-2, and shCRBN, as well as the controls were packaged with pMD2.G, pMDLg/pRRE, and pRSV-Rev (Addgene). Briefly, 1.5 μg pMD2.G, 0.9 μg pMDLg/pRRE, 2.1 μg pRSV-Rev, and 5.4 μg shRNA plasmid were co-transfected into HEK293T cells in 100 mm cell culture dish with Lipofectamine 2000 (Invitrogen, 11668500). The lentivirus particles were harvested, and pipetted into cells in the presence of 0.9 μg/mL polybrene (Sigma−Aldrich, H9268). 2 μg/mL puromycin (Sigma−Aldrich, P8833) for knockdown cells post inoculation to select positive infected-cells. The target sequence of shRNAs was as follows, shFTO-1−TCACGAATTGCCCGAACATTA, shFTO-2−CGGTTCACAACCTCGGTTTAG, and shCRBN−GCTTGCAACTTGAATCTGATA.

2.12. In cellulo coimmunoprecipitation

HEK293T cells stably transfected with Flag-tagged CRBN were plated in a 10 cm dish and allowed to grow to full confluency. Cells were treated with 1 μmol/L bortezomib (HY-10227, Medchemexpress) and incubated at 37 °C for 1 h. The cells were then treated with either 500 nmol/L QP73 or DMSO and incubated at 37 °C for 8 h. Cells were washed with PBS (2 × 10 mL) and lysed with 400 μL IP Lysis Bulfer (Beyotime, P0013) containing 1 × protease inhibitors. The cells were incubated on ice for 5 min and then harvested by scraping. Lysate was incubated on ice for 5 min and then cleared by centrifugation (12,000×g) at 4 °C for 10 min. Solubilized protein concentration was determined by BCA assay and adjusted to 1 mg/mL in lysis buffer. Adjusted lysate (200 μL) was added to 5 μL Flag antibody at 4 °C overnight, then transferred into 30 μL pre-cleared Protein A/G beads and incubated at 4 °C for 1 h. The supernatant was removed, and the beads were washed with TBST (3 × 300 μL). 1 × Loading buffer (50 μL) was added to the beads and boiled at 100 °C for 10 min. The samples were analyzed by Western blot.

2.13. Proteomic profiling

Cells were washed three times with PBS, and each sample was added 200 μL of SDT lysis buffer (4% sodium SDS, 100 mmol/L Tris-HCl, 0.1 mol/L dithiothreitol, pH 7.6). Cells were lysed by sonication and heating at 95 °C for 10 min. The supernatant was collected by centrifugation at 12,000×g for 10 min and used for proteomic analysis. The samples were digested at 37 °C overnight using trypsin (1:50 w/w; Promega) in 100 mmol/L NH$_4$HCO$_3$ solution. The digested peptides were desalted (3 M Empore) and vacuum centrifuged.

For DIA-MS analysis, the peptides were resolved using 0.1% formic acid and measured using NanoDrop (Thermofisher, USA). Peptides were separated using a home-made micro-tip C18 column (75 mm × 200 mm) on a nanoflow HPLC Easy-nLC 1200 system (Thermo Fisher Scientific), with a 60 min LC gradient at 300 nL/min. Mobile phase A consisted of 0.1% (v/v) formic acid in H$_2$O and phase B consisted of 0.1% (v/v) formic acid in acetonitrile. The gradient was set as follows: 2%−5% B in 0−1 min; 5%−35% B in 1−47 min; 35%−45% B in 47−52 min; 45%−100% B in 52−54 min; 100% B in 54−60 min. Proteomic analyses were performed on a Q Exactive HFX mass spectrometer (Thermo Fisher Scientific). MS parameters were as follows: The MS1 full scan was set at a resolution of 120,000, m/z = 350−1650, AGC target = 3e^6, maximum IT = 100 ms, followed by 40 DIA isolation windows with variable width. The isolation windows were set with 1 Da overlap. The MS2 scans generated by HCD fragmentation at a resolution of 30,000, m/z 200, AGC target = 1e^6 and maximum IT auto. The fixed first mass of MS2 spectrum was set 100.0 m/z. The normalized collision energy (NCE) was set at NCE 27%.

The DIA-NN software (version 1.8.1) was used to analyze DIA MS raw files with default parameters[28], against the human Swiss-Prot database containing 20,610 sequences (downloaded in August 2022). Next, the data matrix was normalized with median centering method for each sample.

The Excel, GraphPad Prism, and GSEA software programs were used for bioinformatic analysis. The visualization of pathway enrichment and the degradation of proteins were plotted in GraphPad Prism. Functional enrichment analysis of differential proteins was performed with Database for Annotation, Visualization and Integrated Discovery (DAVID) (https://david.ncifcrf.gov/)[29], using Gene Ontology Biological Processes, Kyoto Encyclopedia of Genes and Genomes. GSEA analysis was performed with GSEA software[30]. Gene sets were h.all.v2023.2.Hs.symbols.gmt for analysis.

2.14. In vivo xenograft tumor models

Female BALB/c nude mice (4−6-week-old, 16−18 g) were purchased from Beijing HFK Bio-Technology. Co., Ltd. All mice experiments were performed according to the institutional ethical guidelines on animal care and were approved by the Institutional Animal Care and Use Committee at Yanxuan Biotechnology (Hangzhou) Co., Ltd. [SYXK (Zhe) 2021-0043]. Housing conditions of dark/light cycle 12 h, ambient temperature 20−26 °C, humidity 40%−60% were applied on mice. All procedures were carried out in strict accordance with the Guide for the Care and Use of Laboratory Animals and the Regulation of the Animal Protection Committee to minimize suffering and injury.

The BALB/c nude mice were assayed in AML subcutaneous xenograft models. 4 × 10^6 NB4 and 2.5 × 10^6 MV4-11 AML cells were collected, and resuspended in 100 μL 50% matrigel membrane matrix (356234, Corning) diluted in RPMI 1640 medium or Iscove's modification of Dulbecco's medium. The cells were implanted subcutaneously into the flanks of BALB/c nude recipient mice on the right sides. Tumor was measured for the short and long diameter using a caliper, and the volume was calculated using Eq. (1):

$$\text{Volume} = (\text{Short} \times \text{Short} \times \text{Large})/2 \tag{1}$$

Drug treatment began when the tumor size was larger than 100 mm^3. QP73 (2.5 and 5 mg/kg) or the control vehicle (10% DMSO, 40% PEG400, 5% Tween80, and 45% saline) were administrated daily by i.p. injection. All mice were euthanized at the endpoint, and tumor tissue was removed for further analysis. The differences in tumor volume and tumor weight between QP73 and control vehicle were analyzed using two-way ANOVA with Dunnett's multiple comparisons test.

3. Results and discussion

3.1. Design of Q-9f/QP73 as a potent PROTAC degrader for FTO

Given that a suitable linker attachment site is crucial for the rational design of PROTAC degraders, we analyzed the structure

of FTO/FB23 complex (PDB code 6AKW) to identify an appropriate linker position on FB23 scaffold (Fig. 1A)[15]. Since the carboxylic acid in FB23 is positioned in a solvent-exposed region in the FTO pocket, chemically modifying this site should minimally hinder the binding of FB23-derived compounds to FTO (Fig. 1B). We then synthesized a series of heterobifunctional PROTAC degraders (Q-9a−Q-9e) composed of the FTO warhead (FB23), an established ligand of the E3 ligase CRBN (thalidomide), and various diamine linkers (Supporting Information Schemes S1 and S2, Fig. 1C).

Next, we evaluated these degraders at 50 and 100 nmol/L in an FTO degradation assay in NB4 cells (Fig. 1D). Unsurprisingly, the diamine linker dramatically impacts FTO degradation. The PROTAC degraders Q-9a−Q-9c, bearing piperidin-4-ylmethanamine, pyrrolidin-3-ylmethanamine, and 7-azaspiro[3.5]nonan-2-amine as linkers, showed weak FTO degradation (Fig. 1C and D). Interestingly, reversing the connecting orientation of the linker of Q-9c yielded Q-9d, which significantly degraded FTO at 100 nmol/L in NB4 cells. Q-9e, bearing 4,4′-bipiperidine, a longer linker than the linker of Q-9d, was inactive for FTO degradation at 100 nmol/L. In contrast to the FTO-targeting PROTAC degraders bearing the semi-rigid diamines linkers, we found that Q-9g−Q-9k-containing commonly-used flexible PEG linkers−did not

exhibit the desired activity for FTO degradation in NB4 cells at 10 μmol/L (Supporting Information Scheme S3, and Fig. S1A and B). Additionally, Q-9d and Q-9f exhibited strong antiproliferative activities in NB4 cells (Fig. S1C and D).

We also used Dac85 as the FTO warhead and found that Q-9f/QP73 exhibited even better FTO degradation than Q-9d (Fig. 1E)[31,32]. Among these FTO PROTAC degraders, 100 nmol/L QP73 decreased FTO abundance by 91% in NB4 cells (Fig. 1C and D). Monitoring the time-course degradation of FTO by 200 nmol/L QP73 showed that QP73-promoted decrease of FTO started after 12 h of treatment and was almost complete after 24 h (Fig. 1F). Moreover, QP73 degraded FTO in NB4 cells in a dose-dependent manner with an estimated DC_{50} (half-maximal degradation) of 34.9 nmol/L (Fig. 1G). Similarly, we observed FTO degradation by QP73 in MV4-11 AML cells (DC_{50} = 65.9 nmol/L) (Fig. S1E). However, the FTO inhibitor Dac85 minimally degraded FTO at 5 μmol/L in NB4 cells (Fig. S1F).

We then tested the inhibitory effects of QP73 on the FTO's demethylation activity. Dac85 inhibited FTO demethylation with an IC_{50} of 0.05 μmol/L in a cell-free dot blot assay, while the IC_{50} of QP73 is 1.79 μmol/L (Fig. S1G). We also determined the interaction of QP73 with FTO and CRBN in a thermal shift assay (TSA). QP73 stabilized the protein folding of FTO and CRBN
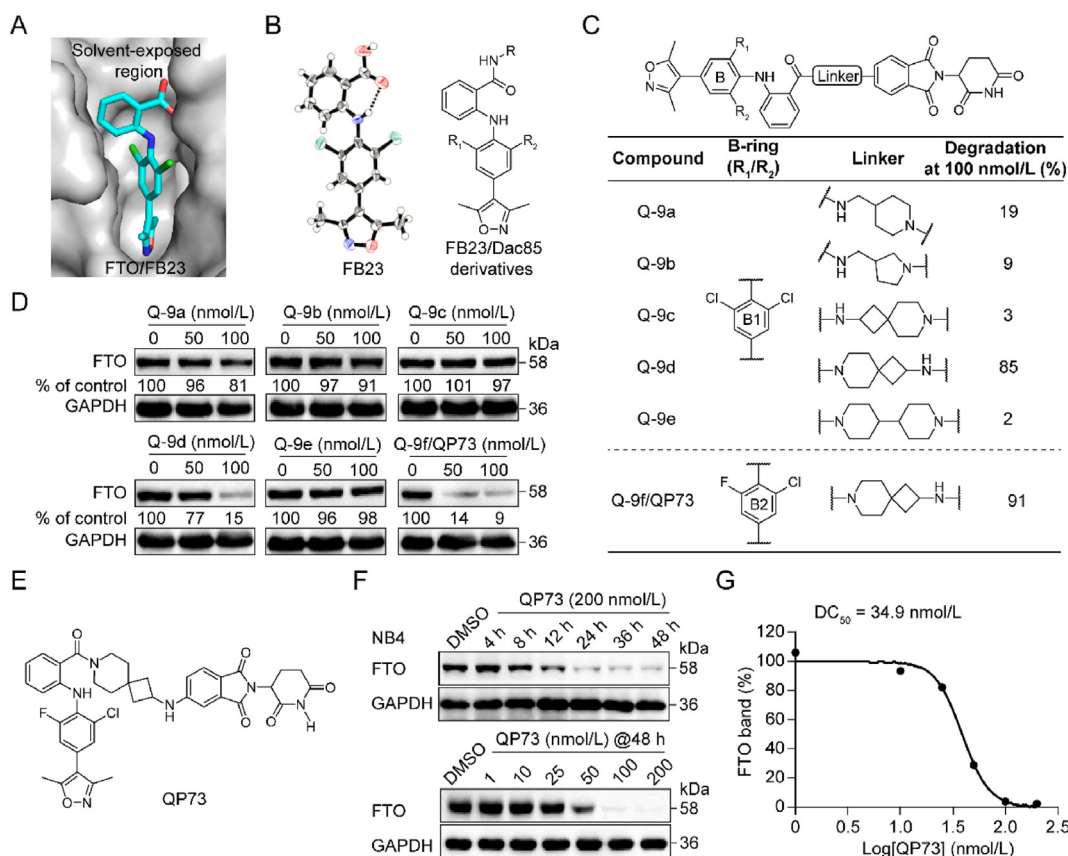

Figure 1 Design and assessment of FTO-targeting PROTAC degraders. (A) Close view of the FTO inhibitor FB23 binding to FTO (PDB code 6AKW). The FTO protein appears as a gray surface and FB23 appears as cyan sticks. (B) Structures of FB23 and the amide derivatives. The X-ray crystal structure of FB23 reveals an intramolecular H-bond. The derived amide will place itself in the solvent-exposed region when binding to FTO. (C) Structures of the FTO PROTAC degraders with different B rings and varying diamine linkers. (D) Western blot images showing FTO degradation in NB4 cells treated with compounds at indicated concentrations for 48 h. The FTO protein was quantified by analyzing band intensity using Image J. (E) Structure of the FTO PROTAC degrader QP73. (F) Immunoblot analysis showing the effects of QP73 on FTO degradation in NB4 cells at indicated time and concentrations. (G) Degradation curve of FTO in NB4 cells treated with QP73.

with a melting temperature change (ΔT_m) of 1.2 and 1.5 °C in the presence of QP73 at a 20-fold molar excess, respectively (Fig. S1H). Taken together, among the designed FTO PROTAC degraders, QP73 is the most potent for decreasing FTO abundance in AML cells.

3.2. QP73 exerts high antileukemic activity by targeting FTO in AML cells

We next assessed the antileukemic activities of QP73 in various AML cell lines with different genetic backgrounds. The FTO PROTAC degrader QP73 exhibited a markedly more potent antiproliferative activity than the FTO inhibitor Dac85. QP73 efficiently inhibited the proliferation of the AML cell lines

with low nanomolar IC_{50} values (12.9−108.1 nmol/L) (Fig. 2A), while the IC_{50} values of Dac85 ranged between 3.4 and 28.4 μmol/L (Fig. 2B). Moreover, QP73 inhibited the clone formation of NB4 cells in a concentration-dependent manner (Fig. 2C). The quantitative PCR analysis showed that QP73 did not affect mRNA levels of FTO at 100 nmol/L in NB4 cells, indicating that QP73 degraded the FTO protein rather than inhibited *FTO* transcription (Supporting Information Fig. S2A). To investigate the target engagement of QP73 in AML cells, we performed a cellular thermal shift assay (CETSA)[15,33]. As expected, QP73 treatment substantially stabilized the FTO protein folding in NB4 and MV4-11 cells (Fig. 2D and Fig. S2B), suggesting that QP73 directly interacted with FTO in AML cells. As a result of FTO degradation, QP73 treatment markedly increased the
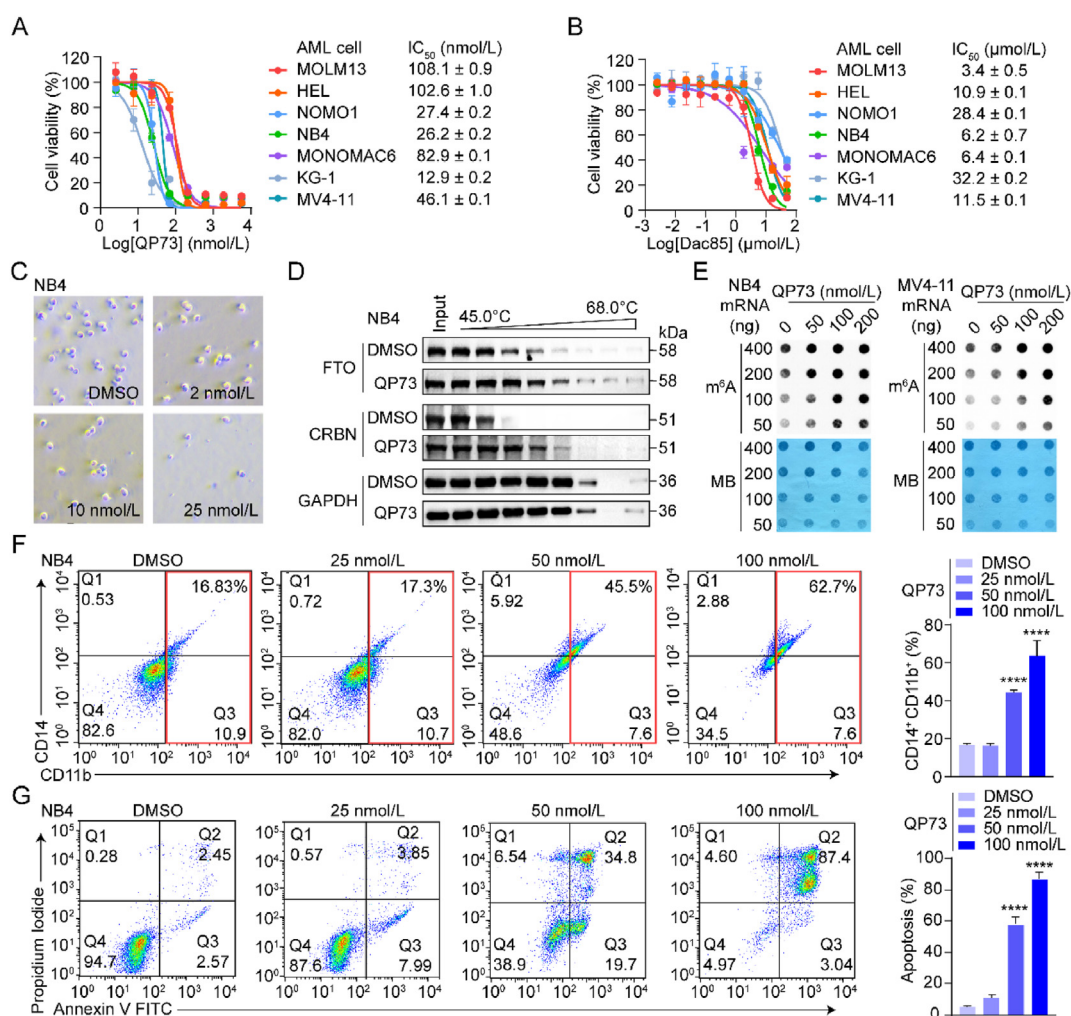

Figure 2 Assessment of antileukemic effects of QP73 in AML cells. (A, B) Inhibitory effects of QP73 (A) and Dac85 (B) on cell viability in seven AML cell lines ($n = 3$). The AML cells were exposed to compounds for 72 h. (C) Representative images of the effect of QP73 on clone formation in NB4 cells. The cells were treated with QP73 at indicated concentrations for 7 days ($n = 3$). (D) Effect of QP73 on the thermal denaturation of the FTO protein in AML cells. CETSA assay was performed on NB4 cell lysis with 50 μmol/L QP73 treated for 30 min. (E) Effect of QP73 on the m^6A abundance on mRNA in NB4 and MV4-11 cells detected in dot blot assay. The AML cells were treated with QP73 at indicated concentrations for 48 h. Methylene blue (MB) is the loading control for the mRNA samples. (F) Effect of QP73 treatment on myeloid differentiation in the presence of 200 nmol/L all-*trans*-retinoic acid (ATRA) in NB4 cells ($n = 3$). The cells were exposed to QP73 at indicated concentrations for 48 h. The positive cells for CD14 and CD11b staining were quantified by flow cytometry. (G) Apoptosis quantification in NB4 cells treated with QP73 at indicated concentrations for 48 h ($n = 3$). The PI- and Annexin V-positive cells were quantified by flow cytometry. Statistical differences were analyzed using one-way ANOVA with Dunnett's multiple comparisons test (F, G). Data are presented as mean ± SD (error bars). ****$P < 0.0001$.

m^{6}A abundance on mRNA in a dose-dependent manner in NB4 and MV4-11 cells (Fig. 2E).

It has been established that FTO inhibited the differentiation of all-*trans*-retinoic acid (ATRA)-treated leukemia cells, and either *FTO* gene knockdown or pharmacological inhibition of FTO promoted the ATRA-induced myeloid differentiation[15,19]. To determine whether the FTO PROTAC degrader similarly regulates the differentiation of AML cells, we performed flow cytometry analysis and found that combining QP73 with ATRA also significantly promoted myeloid differentiation in NB4 and MV4-11 cells (Fig. 2F and Fig. S2C). Additionally, we evaluated the effects of QP73 on cell apoptosis in NB4 cells. QP73 induced cell apoptosis in a concentration-dependent manner after 48 h of treatment (Fig. 2G and Fig. S2D). These results indicate that QP73 exhibited strong antileukemic activities by targeting FTO in AML cells.

3.3. QP73 degrades FTO through a CRBN-dependent proteasomal degradation mechanism

We wondered whether the decrease of FTO abundances induced by QP73 depends on PROTAC-mediated degradation in AML cells. First, we found that pretreating NB4 cells with proteasome inhibitors (bortezomib and MG115) and the neddylation inhibitor (pevonedistat) completely abolished QP73-promoted FTO degradation, suggesting a proteasomal- and neddylation-dependent PROTAC-induced FTO degradation (Fig. 3A). Then, pretreating NB4 cells with CRBN ligands (lenalidomide and pomalidomide) rescued FTO degradation by QP73, indicating a CRBN-dependent mechanism of QP73-promoted FTO degradation (Fig. 3B).

Additionally, treating NB4 cells with 20 μmol/L of lenalidomide substantially weakened the inhibitory effect of QP73 on proliferation in AML cells (Fig. 3C). Similarly, knocking down *CRBN* reduced the sensitivity of NB4 cells to QP73 treatment (Fig. 3D). In line with this observation, QP73 treatment of *CRBN* knockdown AML cells resulted in no FTO degradation (Fig. 3E). We also synthesized QP73N, bearing an isopropyl group to block binding to CRBN, as a negative control (Supporting Information Fig. S3A). QP73N did not affect FTO abundance or cell viability in NB4 and MV4-11 cells (Fig. S3B and C).

We performed *in cellulo* coimmunoprecipitation assay and found that FTO coimmunoprecipitated with Flag-CRBN in HEK293T cells in the presence of QP73 (Fig. 3F), indicating that QP73 participated in the interaction with CRBN and FTO in a ternary complex. Indeed, the FTO abundance also influenced the antiproliferative effect of QP73, since *FTO*-knockdown NB4 cells became resistant to QP73 treatment (Fig. 3G and H). We are aware that structural illustrations of the ternary complex of FTO-QP73-CRBN are required for understanding the mechanism of actions and achieving a rational design of more potent FTO PROTAC degraders in future studies. Collectively, these data demonstrate that QP73 exerted its antileukemic activities by inducing the formation of a ternary complex with FTO and CRBN to initiate a ubiquitin−proteasome system-dependent FTO degradation.

3.4. QP73 exerts antileukemic effects by modulating FTO signaling pathways

To investigate the effects of QP73 on global protein abundance in AML cells, we performed timsTOF Pro-label free proteomics and
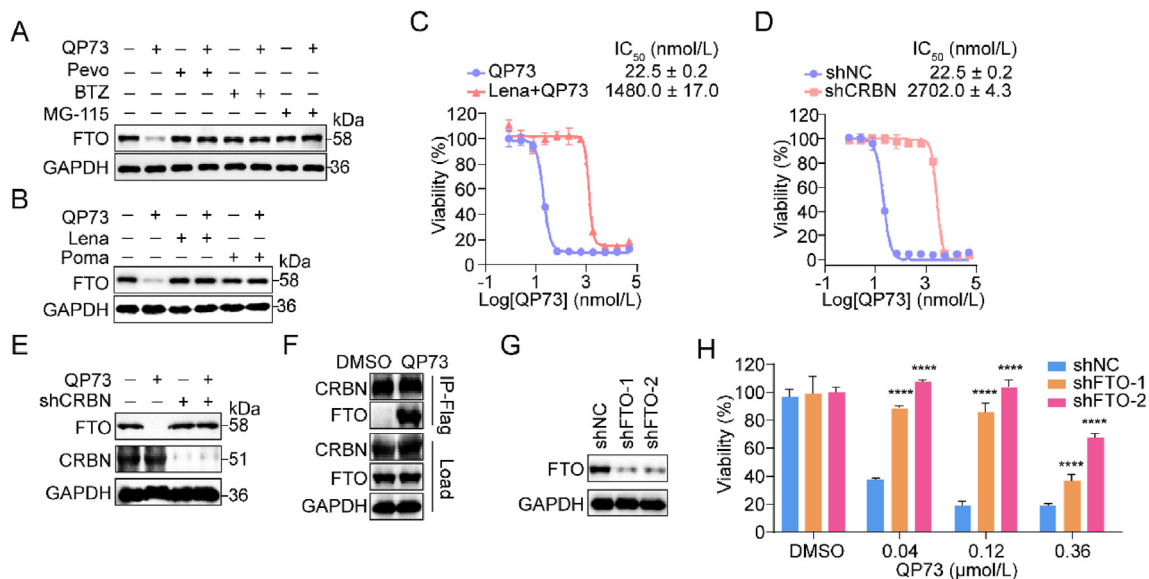

Figure 3 QP73-mediated FTO degradation in a ubiquitin−proteasome pathway. (A) Effect of pevodenist (Pevo, 500 nmol/L), bortezomib (BTZ, 1 μmol/L), and MG-115 (1 μmol/L) on QP73 (100 nmol/L)-mediated FTO degradation in NB4 cells detected in immunoblot analysis. (B) Effect of lenalidomide (Lena, 10 μmol/L) and pomalidomide (Poma, 10 μmol/L) on QP73 (100 nmol/L)-mediated FTO degradation tested in immunoblot analysis. (C) Effect of lenalidomide (20 μmol/L) on QP73-induced antiproliferation in NB4 cells pretreated for 1 h. (D) Effect of QP73 on cell viability in *CRBN* knockdown NB4 cells. (E) Effect of *CRBN* knockdown on QP73-mediated FTO degradation in NB4 cells detected in immunoblot analysis. *CRBN*-knockdown NB4 cells were treated with QP73 (100 nmol/L) for 48 h. (F) Immunoblot analysis showing coimmunoprecipitation of FTO and overexpressed Flag-CRBN in HEK293T cells in the presence of QP73 (100 nmol/L). The cells were exposed to QP73 for 8 h. (G) Validation of *FTO*-knockdown efficiency in NB4 cells in immunoblot assay. (H) Effect of QP73 on the viability of *FTO*-knockdown and shNC NB4 cells. Statistical difference was analyzed using two-way ANOVA with Dunnett's multiple comparisons test (H). Data are presented as mean ± SD (error bars). ****$P < 0.0001$.

found FTO disappeared in NB4 cells that were treated with 300 nmol/L QP73 for 36 h (Fig. 4A). To reveal the QP73-induced changes in signaling pathways, we performed global gene set enrichment analysis (GSEA)[34]. A set of enriched pathways were significantly dysregulated in NB4 cells treated with QP73 (Fig. 4B). Interestingly, these signaling pathways, including the suppressed pathways of MYC targets V1 and G2M checkpoint, were also observed in *FTO*-knockdown AML cells or in cells treated with a pharmaceutical inhibitor of FTO (Fig. 4C and D)[15,17,19].

In AML cells, either *FTO* knockdown or FTO inhibition increased the protein levels of ASB2 and RARA[5,15], while downregulated CEBPA, MYC, and key glycolytic proteins (such as PFKP and LDHB)[19,35]. In line with the regulatory effects of

Figure 4 The dysregulated cellular pathways mediated by QP73. (A) Effect of QP73 on FTO protein abundance in NB4 cells ($n = 4$). The AML cells were treated with 300 nmol/L QP73 for 36 h and FTO abundance was determined by proteomics. Data are presented as mean $\pm$ SD (error bars). (B) Scattergrams of pathways dysregulated by QP73 treatment, based on GSEA analysis. (C, D) GSEA analysis showing the enriched signaling pathways of MYC TARGETS V1 (C) and G2M CHECKPOINT (D) in QP73-treated NB4 cells. Normalized enrichment score indicates the analysis results across gene sets. The false discovery rate indicates the significance of the enrichment. (E, F) Effect of QP73 (E) and Dac85 (F) on the downstream target genes of FTO in NB4 cells, by immunoblot analysis. The AML cells were treated with QP73 or Dac85 at indicated concentrations for 36 h.

FTO knockdown and FTO inhibition, our FTO PROTAC degrader QP73 at 50 nmol/L remarkably dysregulated these downstream target genes of FTO in NB4 cells (Fig. 4E). Notably, the FTO inhibitor Dac85 at 10 μmol/L showed regulatory effects like those of the FTO PROTAC degrader QP73 at 50 nmol/L (Fig. 4F), indicating that the FTO degrader is superior to the FTO inhibitor for regulation of FTO signaling pathways. It is noteworthy that the off-target effects of the FTO PROTAC degrader QP73 on other m6A modifying proteins and any other pathways affected remain currently underexplored. Therefore, the mechanistic study revealed that QP73 exerted antileukemic effects through highly potent regulation of the key FTO signaling pathways in AML cells.

3.5. Pharmacokinetic studies of QP73

Next, we evaluated the pharmacokinetics of the FTO PROTAC degrader QP73 in CD1 mice and found that QP73 showed encouraging PK results (Table 1). QP73 displayed a half-life ($t_{1/2}$) of 0.50−1.25 h for intravenous (i.v.), intraperitoneal (i.p.), and oral (p.o.) administration at the dosage of 3, 5, and 30 mg/kg. QP73 showed a moderate clearance of 20.1 ± 3.9 mL/min/kg, a maximum concentration (C_{max}) of 2996 ± 441 ng/mL, and an $AUC_{0-\infty}$ of 2541 ± 448 h × ng/mL *via* i.v. administration. In i.p. administration, QP73 exhibited a low clearance of 7.39 ± 0.60 mL/min/kg, a C_{max} of 578 ± 37 ng/mL, and an $AUC_{0-\infty}$ of 3479 ± 588 h × ng/mL. In *p.o.* administration, we observed QP73 exhibited a clearance of 4.55 ± 0.60 mL/min/kg, a C_{max} of 49.1 ± 9.7 ng/mL, and an $AUC_{0-\infty}$ of 237 h × ng/mL.

3.6. QP73 exhibits therapeutic effects in AML xenograft mouse model

To assess the antileukemic efficacy of QP73 *in vivo*, we established a xenograft mouse model by subcutaneously inoculating NB4 cells into female BALB/c nude mice. The mice received an i.p. injection of 2.5 or 5 mg/kg of QP73 or a vehicle daily for 10 days (Fig. 5A). The QP73-treated group had lower tumor volume and tumor weight than the control group (Fig. 5B and C, Supporting Information Fig. S4A), demonstrating the antileukemic therapeutic effect of our FTO PROTAC degrader QP73. Moreover, the treatment did not result in loss of body weight (Fig. 5D), and H&E staining of the organs revealed no pathological damage in QP73-treated mice compared with the control group (Fig. S4B).

To test the effect of QP73 on the degradation of FTO in NB4 cell-derived xenograft tumors, we performed immunoblotting analysis on three tumors randomly collected from the QP73-treated and control groups. QP73 therapy decreased FTO protein levels in tumors (Fig. 5E), which is consistent with the *in vitro* degradation effects. Besides, quantifying the m6A abundance in total RNA of transplanted tumors in dot blot assay revealed that the QP73-treated tumors had higher m6A levels than that in control group, revealing that the antitumor activity of QP73 is correlated with the inhibition of m6A demethylation (Fig. 5F). QP73 treatment also exhibited notable antileukemic efficacy in the MV4-11 AML cell-derived xenograft mouse model, with minimal effects on mice body weight after 29 days of treatment (Fig. S4C). These results demonstrated that QP73 potently suppressed the growth of AML cell-derived xenograft tumors *in vivo*.
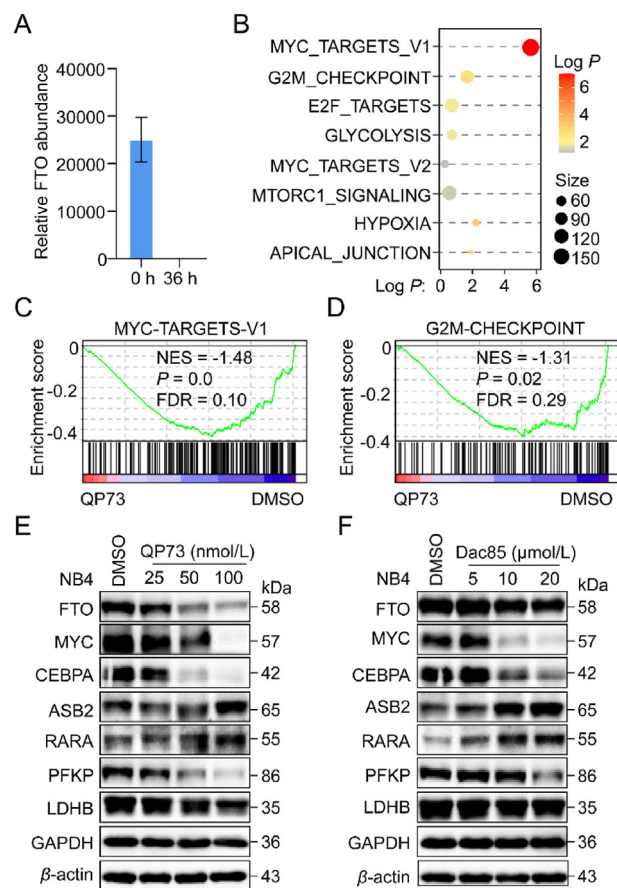
Table 1 The PK profile of QP73.

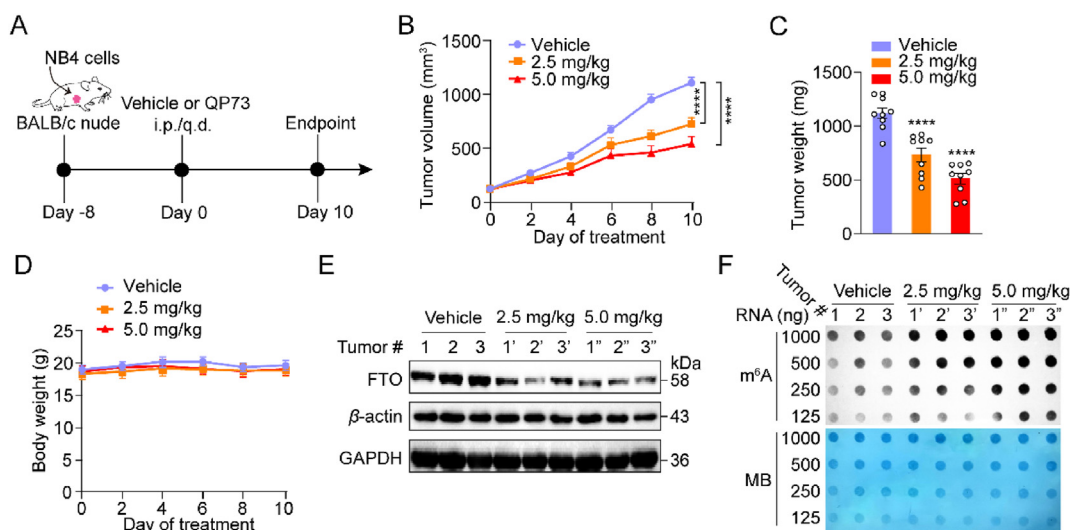| Parameter	i.v. (3 mg/kg)	i.p. (5 mg/kg)	p.o. (30 mg/kg)
$t_{1/2}$ (h)	1.25 ± 0.07	0.50 ± 0	0.50 ± 0
CL_obs (mL/min/kg)	20.1 ± 3.9	7.39 ± 0.60	4.55 ± 0
C_{max} (ng/mL)	2996 ± 441	578 ± 37	49.1 ± 9.7
AUC_{0-t} (h × ng/mL)	2532 ± 445	3201 ± 507	200 ± 36
$AUC_{0-\infty}$ (h × ng/mL)	2541 ± 448	3479 ± 588	237 ± 0

Figure 5 Antileukemic effects of QP73 in AML xenograft tumor models. (A) Schematic diagram of *in vivo* antileukemia test of QP73 on BALB/c nude mice. The mice were administrated by an i.p. injection of 2.5 or 5 mg/kg of QP73 or a vehicle. (B) Tumor growth curves of mice bearing human NB4 cells ($n = 9$). Dots represent the mean tumor volume ± standard error of the mean. (C) NB4 cell-derived xenograft tumor weight. (D) Body weight of mice bearing human NB4 cell-derived tumors. (E) Effect of QP73 on the FTO protein levels in NB4 cell-derived xenograft tumors. (F) Effect of QP73 on m6A abundances in total RNA extracted from NB4 cell-derived xenografted tumors. Differences in tumor volume and tumor weight between groups were analyzed using two-way ANOVA with Dunnett's multiple comparisons test (B, C). Data are shown as mean ± SEM (error bars). ****$P < 0.0001$.

4. Conclusions

The discovery of FTO as the first m6A demethylase introduced a new dimension to gene expression regulation—RNA epigenetics. Targeting the regulatory m6A modifying FTO protein with chemical inhibitors has exerted promising antileukemic effects. We and others developed a series of highly selective and potent inhibitors of FTO using structure-based rational design and high-throughput screening. These inhibitors exerted antileukemic effects by blocking the catalytic demethylation of FTO in AML cells. Although very few inhibitors also decreased FTO abundance in AML cells, the impact of FTO degradation on antileukemic effects remained unknown.

Our demonstration of the first potent FTO-targeting PROTAC degrader QP73 opens a new avenue in modulating RNA epigenetics for antileukemia drug discovery. QP73 potently induced FTO degradation in a time- and dose-dependent manner in AML cells. Notably, QP73 suppressed cell viability broadly in a panel of AML cell lines, and displayed a remarkably improved (100- to 1000-fold) antiproliferative activity compared with the FTO inhibitor Dac85. Similar to the FTO inhibitors, the FTO PROTAC degrader QP73 induced AML cell apoptosis in a concentration-dependent manner and combining QP73 with ATRA considerably promoted myeloid differentiation in AML cells. Mechanistically,

QP73-induced FTO degradation highly depended on the CRBN ligase and the ubiquitin−proteasome system. Quantitative proteomics analysis revealed that QP73 treatment resulted in complete FTO degradation and exerted antileukemic effects by dysregulating the key signaling pathways mediated by FTO in AML cells. In the mouse model, QP73 significantly inhibited the growth of AML cell-derived xenograft tumors.

Given that the C-terminal domain and non-catalytic function of FTO might also significantly contribute to tumor cell viability[36], the FTO ROTAC degrader QP73 entirely erased the FTO protein, leading to loss of functions of both the C-terminal domain and the non-catalytic activity. So, it is unsurprising that the FTO PROTAC degrader is superior to the FTO inhibitor in antiproliferative activity. On the other hand, there is still plenty of room to improve the inhibitory activities of the FTO inhibitors in future studies. So, it is noteworthy that our FTO degrader QP73 displays advantages in antiproliferation in AML cells, which could not weaken the potential application of the FTO inhibitors for antileukemia drug discovery.

In summary, QP73 represents the first FTO PROTAC degrader with potent *in vivo* antileukemic effects. Our development of FTO degraders will tremendously enrich available chemical tools for elucidating the biology of m6A modification and the non-catalytic functions of FTO. To expand the application of PROTAC to the

field of RNA epigenetics for antileukemia drug discovery, the ALKBH5-targeting PROTAC degradation will be similarly explored on the basis of ALKBH5 inhibitors[11,37].

Author contributions

Lu Liu: Writing − original draft, Validation. Yuanlai Qiu: Methodology. Yuying Suo: Methodology. Siyao Tong: Methodology. Yiqing Wang: Investigation. Xi Zhang: Investigation. Liang Chen: Investigation. Yue Huang: Funding acquisition. Huchen Zhou: Funding acquisition. Hu Zhou: Investigation. Ze Dong: Writing − original draft, Investigation. Cai-Guang Yang: Writing − review & editing, Project administration.

Conflicts of interest

Lu Liu, Yuanlai Qiu, Siyao Tong, Ze Dong, and Cai-Guang Yang are named inventors of pending patent applications (CN 202410173007.7, to the Chinese Patent Office) related to the work described.

Appendix A.   Supporting information

Supporting information to this article can be found online at https://doi.org/10.1016/j.apsb.2024.07.016.

References

1. He C. Grand challenge commentary: RNA epigenetics?. *Nat Chem Biol* 2010;**6**:863−5.
2. Jia G, Fu Y, Zhao X, Dai Q, Zheng G, Yang Y, et al. *N*6-Methyladenosine in nuclear RNA is a major substrate of the obesity-associated FTO. *Nat Chem Biol* 2011;**7**:885−7.
3. Roundtree IA, Evans ME, Pan T, He C. Dynamic RNA modifications in gene expression regulation. *Cell* 2017;**169**:1187−200.
4. Frye M, Harada BT, Behm M, He C. RNA modifications modulate gene expression during development. *Science* 2018;**361**:1346−9.
5. Li Z, Weng H, Su R, Weng X, Zuo Z, Li C, et al. FTO plays an oncogenic role in acute myeloid leukemia as a N^6-methyladenosine RNA demethylase. *Cancer Cell* 2017;**31**:127−41.
6. Deng X, Qing Y, Horne D, Huang H, Chen J. The roles and implications of RNA m^{6}A modification in cancer. *Nat Rev Clin Oncol* 2023;**20**:507−26.
7. Zhou LL, Xu H, Huang Y, Yang CG. Targeting the RNA demethylase FTO for cancer therapy. *RSC Chem Biol* 2021;**2**:1352−69.
8. Huang Y, Xia W, Dong Z, Yang CG. Chemical inhibitors targeting the oncogenic m^{6}A modifying proteins. *Acc Chem Res* 2023;**56**:3010−22.
9. Lai GQ, Zhou LL, Yang CG. RNA methylation m6A: a new code and drug target?. *Chin J Chem* 2020;**38**:420−1.
10. Zhou LL, Yang CG. Targeting epitranscriptomic proteins for therapeutic intervention. *Biochemistry* 2020;**59**:125−7.
11. Gu J, Xu J, You Q, Guo X. Recent developments of small molecules targeting RNA m6A modulators. *Eur J Med Chem* 2020;**196**:112325.
12. Chen B, Ye F, Yu L, Jia G, Huang X, Zhang X, et al. Development of cell-active *N*6-methyladenosine RNA demethylase FTO inhibitor. *J Am Chem Soc* 2012;**134**:17963−71.
13. Huang Y, Yan J, Li Q, Li J, Gong S, Zhou H, et al. Meclofenamic acid selectively inhibits FTO demethylation of m6A over ALKBH5. *Nucleic Acids Res* 2015;**43**:373−84.
14. Yan C, Zhang Q, Xiao P, Xie X, Li M, Qiu Y, et al. Structure−activity relationships of 2-(arylthio)benzoic acid FTO inhibitors. *Isra J Chem* 2024;**64**:e202300166.
15. Huang Y, Su R, Sheng Y, Dong L, Dong Z, Xu H, et al. Small-molecule targeting of oncogenic FTO demethylase in acute myeloid leukemia. *Cancer Cell* 2019;**35**:677−91.
16. Van Der Werf I, Jamieson C. The yin and yang of RNA methylation: an imbalance of erasers enhances sensitivity to FTO demethylase small-molecule targeting in leukemia stem cells. *Cancer Cell* 2019;**35**:540−1.
17. Su R, Dong L, Li Y, Gao M, Han L, Wunderlich M, et al. Targeting FTO suppresses cancer stem cell maintenance and immune evasion. *Cancer Cell* 2020;**38**:79−96.
18. Sun K, Du Y, Hou Y, Zhao M, Li J, Du Y, et al. Saikosaponin D exhibits anti-leukemic activity by targeting FTO/m6A signaling. *Theranostics* 2021;**11**:5831−46.
19. Su R, Dong L, Li C, Nachtergaele S, Wunderlich M, Qing Y, et al. R-2HG exhibits anti-tumor activity by targeting FTO/m^{6}A/MYC/CEBPA signaling. *Cell* 2018;**172**:90−105.
20. Liu Y, Liang G, Xu H, Dong W, Dong Z, Qiu Z, et al. Tumors exploit FTO-mediated regulation of glycolytic metabolism to evade immune surveillance. *Cell Metab* 2021;**33**:1221−33.
21. Burslem GM, Crews CM. Proteolysis-targeting chimeras as therapeutics and tools for biological discovery. *Cell* 2020;**181**:102−14.
22. Chirnomas D, Hornberger KR, Crews CM. Protein degraders enter the clinic−a new approach to cancer therapy. *Nat Rev Clin Oncol* 2023;**20**:265−78.
23. Bond MJ, Crews CM. Proteolysis targeting chimeras (PROTACs) come of age: entering the third decade of targeted protein degradation. *RSC Chem Biol* 2021;**2**:725−42.
24. He M, Cao C, Ni Z, Liu Y, Song P, Hao S, et al. PROTACs: great opportunities for academia and industry (an update from 2020 to 2021). *Signal Transduct Target Ther* 2022;**7**:181.
25. He S, Dong G, Cheng J, Wu Y, Sheng C. Strategies for designing proteolysis targeting chimaeras (PROTACs). *Med Res Rev* 2022;**42**:1280−342.
26. Peng X, Hu Z, Zeng L, Zhang M, Xu C, Lu B, et al. Overview of epigenetic degraders based on PROTAC, molecular glue, and hydrophobic tagging technologies. *Acta Pharm Sin B* 2024;**14**:533−78.
27. Wang Y, Jiang X, Feng F, Liu W, Sun H. Degradation of proteins by PROTACs and other strategies. *Acta Pharm Sin B* 2020;**10**:207−38.
28. Demichev V, Messner CB, Vernardis SI, Lilley KS, Ralser M. DIA-NN: neural networks and interference correction enable deep proteome coverage in high throughput. *Nat Methods* 2020;**17**:41−4.
29. Sherman BT, Hao M, Qiu J, Jiao X, Baseler MW, Lane HC, et al. David: a web server for functional enrichment analysis and functional annotation of gene lists (2021 update). *Nucleic Acids Res* 2022;**50**:W216−21.
30. Subramanian A, Tamayo P, Mootha VK, Mukherjee S, Ebert BL, Gillette MA, et al. Gene set enrichment analysis: a knowledge-based approach for interpreting genome-wide expression profiles. *Proc Natl Acad Sci USA* 2005;**102**:15545−50.
31. Liu Z, Duan Z, Zhang D, Xiao P, Zhang T, Xu H, et al. Structure−activity relationships and antileukemia effects of the tricyclic benzoic acid FTO inhibitors. *J Med Chem* 2022;**65**:10638−54.

32. Xiao P, Duan Z, Liu Z, Chen L, Zhang D, Liu L, et al. Rational design of RNA demethylase FTO inhibitors with enhanced antileukemia drug-like properties. *J Med Chem* 2023;**66**:9731−52.

33. Molina DM, Jafari R, Ignatushchenko M, Seki T, Larsson EA, Dan C, et al. Monitoring drug target engagement in cells and tissues using the cellular thermal shift assay. *Science* 2013;**341**:84−7.

34. Suo Y, Du D, Chen C, Zhu H, Wang X, Song N, et al. Uncovering PROTAC sensitivity and efficacy by multidimensional proteome profiling: a case for STAT3. *J Med Chem* 2024;**67**:4804−18.

35. Qing Y, Dong L, Gao L, Li C, Li Y, Han L, et al. *R*-2-Hydroxyglutarate attenuates aerobic glycolysis in leukemia by targeting the FTO/m⁶A/PFKP/LDHB axis. *Mol Cel* 2021;**81**:922−39.

36. Song H, Wang Y, Wang R, Zhang X, Liu Y, Jia G, et al. SFPQ is an FTO-binding protein that facilitates the demethylation substrate preference. *Cell Chem Biol* 2020;**27**:283. 91.e6.

37. Lai GQ, Li Y, Zhu H, Zhang T, Gao J, Zhou H, et al. A covalent compound selectively inhibits RNA demethylase ALKBH5 rather than FTO. *RSC Chem Biol* 2024;**5**:335−43.